Development of a 30-kW Class Magnetically Shielded Nested Hall Thruster

IEPC-2019-266

Presented at the 36th International Electric Propulsion Conference
University of Vienna, Austria
September 15–20, 2019

Sarah E. Cusson,[*]
University of Michigan, Ann Arbor, MI 48109

Richard R. Hofer,[†] Dan M. Goebel [‡]
Jet Propulsion Laboratory, California Institute of Technology, Pasadena, California, 91109

Marcel P. Georgin,[§] Alexander R. Vazsonyi,[¶] Benjamin A. Jorns,[‖] Alec D. Gallimore,[**]
and Iain D. Boyd[††]
University of Michigan, Ann Arbor, MI 48109

[*]Ph.D Candidate, Department of Aerospace Engineering, cusson@umich.edu
[†]Supervisor, Electric Propulsion Group
[‡]Senior Research Scientist, Propulsion, Materials and Thermal Engineering Section
[§]Ph.D. Candidate, Applied Physics Program
[¶]Ph.D. Candidate, Department of Aerospace Engineering
[‖]Assistant Professor, Department of Aerospace Engineering
[**]Robert J. Vlasic Dean of Engineering, the Richard F. and Eleanor A. Towner Professor of Engineering, and Arthur F. Thurnau Professor of Aerospace Engineering
[††]James E. Knott Professor, Department of Aerospace Engineering

An overview of the design process, acceptance testing, and initial performance mapping of the N30, a 30-kW class dual-channel magnetically shielded Hall thruster, is presented. The thruster was developed by the University of Michigan in collaboration with the Jet Propulsion Laboratory. This new thruster provides a testbed for nested Hall thruster physics and technology development. The inner channel of the N30 shares the geometry, anode/gas distributor, and near-field magnetic field shape with the H9, a 9 kW magnetically shielded Hall thruster. This allows for direct comparisons between the inner channel and the H9. The outer channel also provides magnetic shielding up to 800 V, with a total discharge power of 33 kW in dual channel mode. A new lanthanum-hexaboride cathode was designed to enable high current operation while still fitting the form factor of the H9. The thruster passed acceptance testing with inner and outer anode flow variations of 4.0% and 8.4% at high flow rates respectively. The magnetic field testing demonstrated 50% margin on the nominal strength. Characterization of the inner channel indicates a peak thrust of 451 mN and peak efficiency of 65% at 600 V, and peak specific impulse of 2830 seconds at 800 V. Performance testing is on-going for other firing configurations and all results thus far indicate state-of-the-art performance.

Nomenclature

$\langle() \rangle$	= Average
$\delta()$	=Deviation from average
I_d	= Discharge current
I_{sp}	= Specific impulse
$P2P$	= AC peak-to-peak
p	= Pressure
P_d	= Discharge power
P_{mag}	= Magnet power
V_d	= Discharge voltage

I. Introduction

Although state of the art electric propulsion systems flying today are currently limited to discharge powers less than 4.5 kW, there are a number of enabling, near and far-term architectures that could be realized if the available power could be expanded to 100s of kWs.[1–3] These missions include Mars and Moon cargo missions[4–6], human missions to Phobos and Deimos[7], and missions to near-Earth asteroids[8], among others. In fact, a recent study also identified a viable architecture for a solar electric crewed mission to Mars.[9] NASA views the development of these higher power electric propulsion systems as critical for its mission and has supported them through the NextSTEP technology development program and the Advanced Electric Propulsion System (AEPS).[1,10]

While there are a number of alternative solutions currently being explored toward this end,[11,12] the University of Michigan, in conjunction with NASA Glenn Research Center, NASA Jet Propulsion Laboratory, the Air Force Research Laboratory, and Aerojet Rocketdyne, has investigated the concept of nested Hall thrusters as a mechanism for achieving the high powers necessary. Nested Hall thrusters (NHTs) concentrically nest multiple annular discharges together. This allows high efficiency and thrust-to-power ratios at very high powers (>50 kW) with a lower specific mass and expanded throttling range compared to their single channel counterparts.[13] At the same time, they leverage the nearly five decades of flight heritage and maturity of single channel Hall thrusters. Previous nested Hall thrusters have proved the concept at moderate and very high powers,[14,15] as well as provided testbeds for investigations into the interactions of neutrals and magnetic fields between channels.[16,17] Additionally, they have been shown to have comparable efficiency to single-channel Hall thrusters, demonstrated at thermal steady state up to 72 kW, set the record for thrust for Hall thrusters, and operated up to 100 kW.[18,19] However, these devices are still a nascent technology with unanswered fundamental questions about their operation. For instance, the interaction of the two plasma streams in close proximity and its impact on thruster behavior remains an open question. None of the previous thrusters built have a single channel counterpart for any of their channels making it difficult to de-convolve and compare their multi- versus single-channel operation. Additionally, and perhaps of greater importance, none of these thrusters have implemented magnetic shielding. Magnetic shielding shapes the magnetic field in a way that increases the lifetime up to three orders of magnitude.[20–23]

In order to continue the development and exploration of this technology, the University of Michigan, in collaboration with the Jet Propulsion Laboratory, has developed a new 30-kW class nested Hall thruster, the N30. This thruster is a two-channel, magnetically shielded, nested Hall thruster. The power level was chosen based on the abilities of ground testing facilities and to enable comparison to the H9 thruster. By implementing the magnetic shielding field topography, we not only explore the ability for nested Hall thrusters to achieve lifetimes comparable to their state-of-the-art single channel counterparts, but also provide another platform to research the implications of this relatively new advancement in the field. Additionally, the inner channel of this device shares geometry and design heritage with the H9, a 9-kW magnetically shielded Hall thruster.[24,25] This allows for a systematic investigation between single-channel Hall thrusters, single-channel operation in a nested Hall thruster, and multi-channel operation. Thus, we are better able to study the implications of multiple plasma discharges in close proximity. To further enable both of these goals, a new high-current cathode was developed to supply discharge current for the H9 and this N30.

The goal of this work is to present the design and some initial testing of this new NHT. As such, we organize the paper as follows: first, we discuss the design goals, requirements, and the component features. Major challenges presented with the respect to the design include anode uniformity, magnetic field design, and the need to correct for cross-coupling effects in the magnetic field design. We also

discuss the operating envelope and reference firing conditions in this section. We then present the acceptance testing results, including the anode flow uniformity, magnetic field mapping, and initial firing. Next, we present initial testing results including thrust, oscillation mapping, and evidence of magnetic shielding. Finally, we make concluding remarks and discuss future work for the thruster.

II. Design Process

In this section, we first discuss the history of development leading to the N30 and then present the overall design of the thruster. Then, we present the overall goals and objectives of the N30, the derived design requirements, and component features.

A. Development History

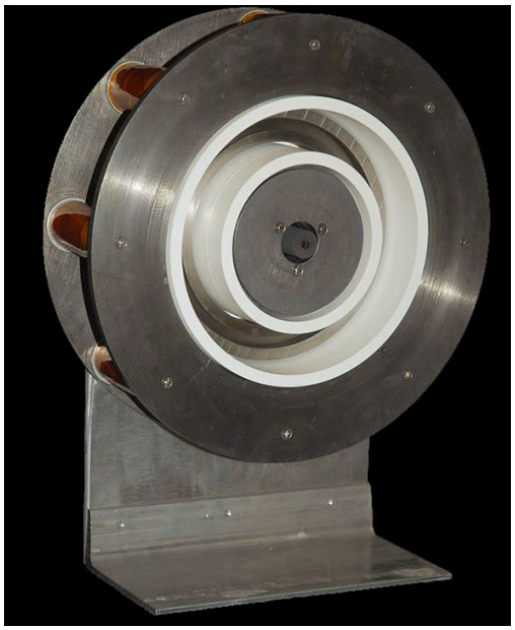

Fig. 1 A photo of the H6 after manufacturing. Taken from Reid.[26]

The N30 is the latest thruster in a long line of development history that began with the H6. The H6 is a 6-kW Hall thruster designed in 2006 with the purpose of creating a uniform testbed for Hall thruster physics and development research in the United States.[27] The thruster was a joint development project between the Air Force Research Laboratory, NASA's Jet Propulsion Laboratory (JPL), and the University of Michigan, with three thrusters fabricated in total. Many features that were included in the H6 design were carried through to other thrusters in this series, including a plasma lens magnetic field topography,[28–30] a centrally-mounted LaB_6 cathode,[31–34] and a high uniformity gas distributor and anode[35]. All of these features combined culminated in the demonstration of new milestones in performance including 401 mN of thrust, 1950s of total specific impulse, and 64% total efficiency at the nominal, 6-kW, 300 V condition. When the discharge voltage was raised to 800 V, total efficiencies of 70% were achieved. The development of this thruster led to numerous journal and conference proceedings as well as doctoral dissertations. As a laboratory testbed, it also facilitated a new understanding of thruster operation at high specific impulse and helped guide the development of so-called magnetic shielding.

In 2011, JPL retrofitted their H6 to incorporate magnetic shielding, designated the H6MS. The physics of magnetic shielding emerged from a combination of experimental observations and numerical investigations. During a 10,400 h wear test of the XR-5 Hall thruster by Aerojet Rocketdyne, no appreciable erosion occurred from 5,600 h onward.[36] JPL subsequently performed numerical simulations that revealed the physics behind this low-erosion state and critically, demonstrated the effect was not due to vacuum facility interactions.[22] The subsequent retrofit of the H6 Hall thruster verified the physics of magnetic shielding through simulation and experiments, demonstrating a reduction in discharge chamber erosion of three orders of magnitude.[20,21,23,37] This reduction in erosion came with only a small change in performance.[21]

Following the success of the H6MS, as well as numerous research studies, a collaborative effort to design a new testbed for Hall thruster research in the United States began in 2016. This effort was led by JPL in collaboration with the University of Michigan and the Air Force Research Laboratory.[24] This new thruster, the H9, shared many critical components with the H6MS, including the discharge chamber geometry and anode design. Thus, research performed on the thruster could still be compared to the H6 variants. However, because this thruster was designed from conception to be magnetically shielded, it was not limited by the same constraints that the retrofit of the H6 was. Additionally, this thruster was designed for high-I_{sp} operation at 9 kW and 800 V. At the comparable 300 V, 6 kW condition, this thruster produced 384 mN of thrust and 1970 s of total specific impulse all at 62% total efficiency.[25] These numbers are within 1.5% of its counterpart, the H6MS, all while achieving a higher degree of shielding.[21]

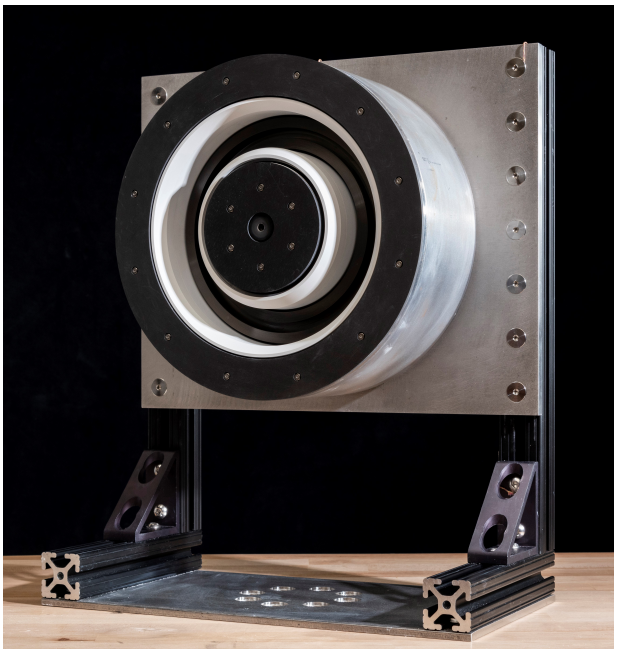

(a) A photo of the H9 Hall thruster.

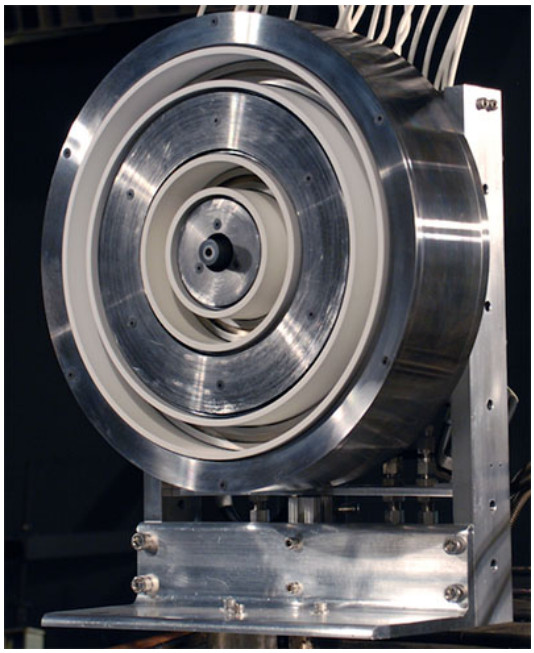

(b) A photo of the X2 taken from Liang.[14]

Beginning in 2009, the development of nested Hall thrusters (at the University of Michigan) began. The first nested Hall thruster in this line was the X2, a two-channel NHT, led by the University of Michigan in collaboration with the Air Force Research Laboratory.[14,38,39] This thruster, capable of discharge powers up to 10 kW, was developed as a proof-of-concept for nesting multiple channels together.[39] Because nested Hall thrusters have a variable discharge area, they enable a wider operational envelope. For instance, the X2 confirmed operation between 1000 and 3000 s of I_{sp} all at 6 kW by switching the firing configurations.[39] This allows the operator to choose their operating mode: high specific impulse or high thrust. Alternatively, nested Hall thrusters enable a high efficiency, high specific impulse mode over a much wider range of operating powers. This is particularly critical for deep space missions where available power changes depending on the spacecraft's distance to the sun. Additionally, some initial work on the X2 indicated that dual channel operation may lead to enhanced performance compared to the sum of single channel operation on nested Hall thrusters.[14,16] Finally, the X2 proved that nested Hall thrusters could run off a single centrally-mounted cathode.

Upon validation of the nested configuration, work began on the development of a much higher power

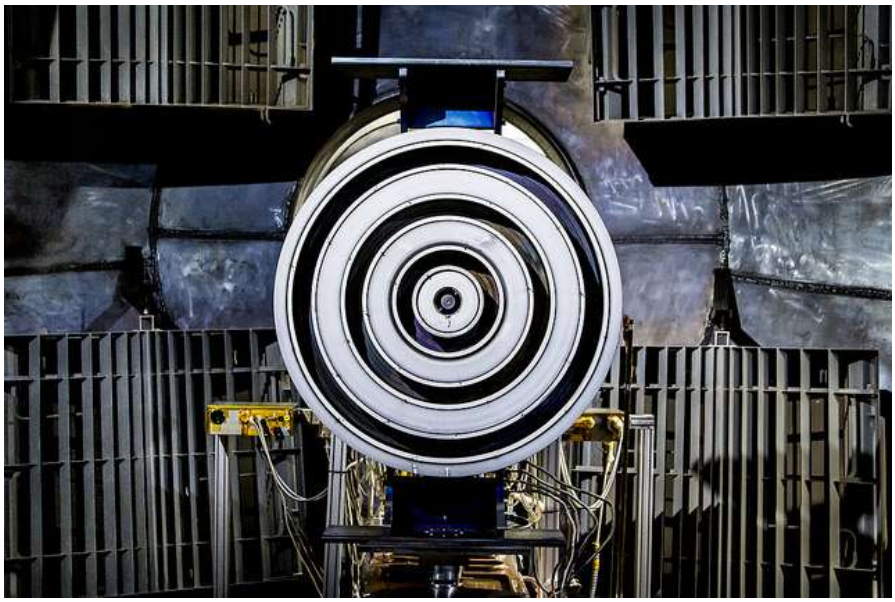

Fig. 3 The X3 Hall thruster (taken from Hall)[40]

nested Hall thruster. This thruster, the X3, was a joint development project between the University of Michigan, the Air Force Research Laboratory, JPL, and NASA's Glenn Research Center.[15,40] The X3 is a three-channel NHT and was designed for operation up to 200 kW. The scaling of each channel is more similar to the H6 family than the X2. This thruster incorporated the magnetic lens topography on NHTs and continued the validation of the NHTs for high-power electric propulsion. Testing of this thruster is ongoing with the X3 being selected as part of NASA's NextSTEP technology development program.[10] During the NextSTEP program, the X3 Hall thruster demonstrated the highest power (102 kW), highest discharge current (247 A), highest thrust (5.4 N) ever produced by a Hall thruster, and achieved thermal steady state at 72 kW.[18,19] These results helped demonstrate and validate the technology is relevant to the type of missions discussed earlier.

Throughout the process of X2 and X3 testing, certain limitations of these thruster emerged. First and foremost, since their development took place before the advancement of magnetic shielding, neither have incorporated this lifetime extending technology. Since most high-power missions under consideration are deep space, the demonstration of this magnetic field configuration on NHTs is critical. The NextSTEP program, for example, ultimately has the goal of demonstrating >10000 h of operation. While an official lifetime has not been stated, simulations indicate the X3 boron nitride will have eroded 10 mm by 10000 h.[41,42] Moreover, the HERMeS thruster was developed with a 50 kh requirement, which is more in line with most deep space missions.[43] Additionally, throughout testing, we uncovered many ways in which the channels interact with each other such as neutrals emanating from one channel impacting other channels through ingestion and acceleration region location movement, magnetic field interactions, and oscillation behavior changes depending on firing configuration.[14–18] However, since no channel on either thruster has a single channel counterpart, it is difficult to deconvolve the exact implications of nesting channels together. Understanding these implications is critical to their development towards flight. As such, in 2017, the University of Michigan, in collaboration with JPL and supported by the NASA Space Technology Research Fellowship, began development of a third nested Hall thruster, the N30. A picture of the thruster and cathode after manufacturing can be seen in Fig. 4. The details of the objectives, specifications, and component features are elaborated

upon in the following sections.

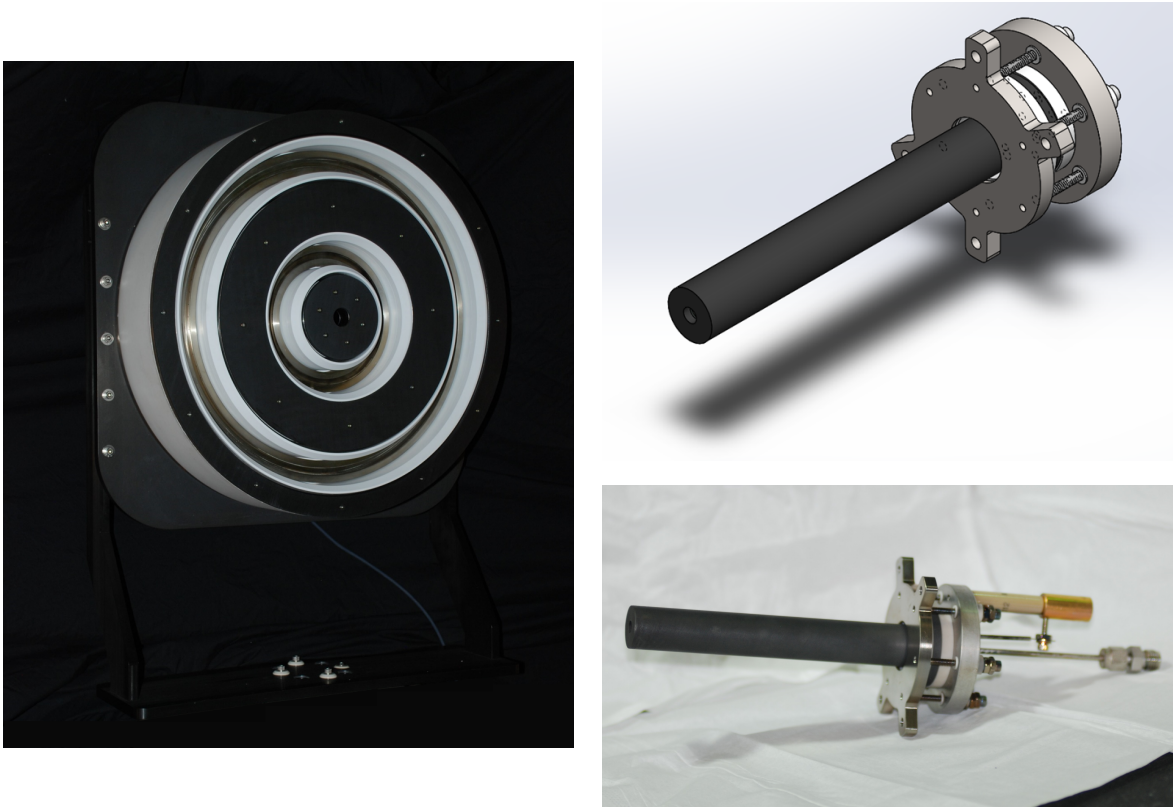

Fig. 4 Left - A picture of the N30 after manufacturing before initial plasma. Right - The model (top) and a picture (bottom) of the new 60 A LaB_6 cathode designed for the thruster after initial testing.

B. Purpose and Objectives

The main objective of the N30 was to continue the development of nested Hall thrusters towards their path to flight as well as provide a testbed for thruster physics and developments in technology. With these high level goals in mind, the specific objectives of the device were to:

- Implement a magnetic circuit that provides magnetic shielding up to 800 V in any firing configuration,
- Provide a high-power (25-50 kW), high specific impulse (up to 3000 seconds) laboratory nested Hall thruster capable of being tested at facilities in the United States at relevant pressures (less than 20μTorr),
- Provide a mechanical design that is simple and flexible such that it can accommodate various diagnostics and potential hardware changes,
- Have the inner channel have an identical geometry and a similar magnetic field shape to a well benchmarked single channel thruster in order to study channel interactions and the differences between single channel and nested Hall thrusters,
- Provide a testbed for NHT lifetime studies; specifically, be able to investigate if magnetic shielding on nested Hall thrusters achieves the same reduction in channel erosion as well as investigate pole erosion of shared poles.

C. Requirements

The design requirements for the N30 are derived from the purpose and objectives listed above. One of the main goals of the N30 is for the inner channel to be as similar to the H9 design as possible such that results between the two thrusters are easily comparable.[24] With this in mind, there are many similarities between the N30 inner channel and the H9. These include identical discharge chamber geometries (mid-channel diameter, channel width, and channel length), an identical anode/gas distributor design, and an internal (to the discharge chamber) magnetic field shape that is nearly identical. Due to differences in the surrounding magnetic material environment, it is impossible for these fields to be identical in the far field (outside of the discharge chamber).

As with the H9, a segmented discharge channel with replaceable rings near the exit region was implemented for both channels to enable future research into material selection. Additionally, there were several requirements for the outer channel and the thruster as a whole. Some thruster-wide requirements include graphite pole covers to mitigate pole erosion[44], a magnetic circuit that provides dual-channel magnetic shielding as well as the ability to operate in single channel and dual channel modes, a consideration for the thermal environment of the thruster to enable high-power dual channel operation, and a single, high-current LaB_6 hollow cathode. The cathode design was further restricted to ensure that it could be used on both the H9 and the NHT in order to eliminate cathode changes as a difference in operation. Finally, there were two main requirements for the outer channel: (1) proper scaling to ensure high-specific impulse (same as the inner channel) operation and (2) a anode/gas distributor design that was similar to the inner channel.

Table 1 Reference Firing Conditions for the N30.

Inner Voltage (V)	Inner Current (A)	Inner Power (kW)	Outer Voltage (V)	Outer Current (A)	Outer Power (kW)	Total Power (kW)
300	15	4.5	300	38.9	11.7	16.2
300	20	6	300	51.8	15.5	21.5
400	15	6	400	38.9	15.5	21.5
500	15	7.5	500	38.9	19.4	27.0
600	15	9	600	38.9	23.3	32.3
800	11.25	9	800	29.2	23.3	32.3

Table 1 details the matrix of Reference Firing Conditions (RFCs) used to benchmark performance. There exist 18 reference firing conditions. The first six conditions in the table (first three columns) are for the inner channel operating alone and are identical to the H9 RFCs.[24] The next six (columns four to six) are for the outer channel operating alone. They are scaled from the inner channel RFCs to maintain the same current density among the two channels. Finally, the last six conditions are dual channel operation and are simply the summation of the inner channel operating alone and the outer channel operating alone. The total power for these six conditions is listed in the last column of the table.

Figure 5 depicts the full operational envelope for the N30. This operational envelope is estimated from experience with the H6, H6MS, H9 and HERMeS Hall thrusters.[24,43,45,46] Similar to the H9, the maximum possible combined (inner and outer channel) thrust is estimated to be 2.0 N at a discharge

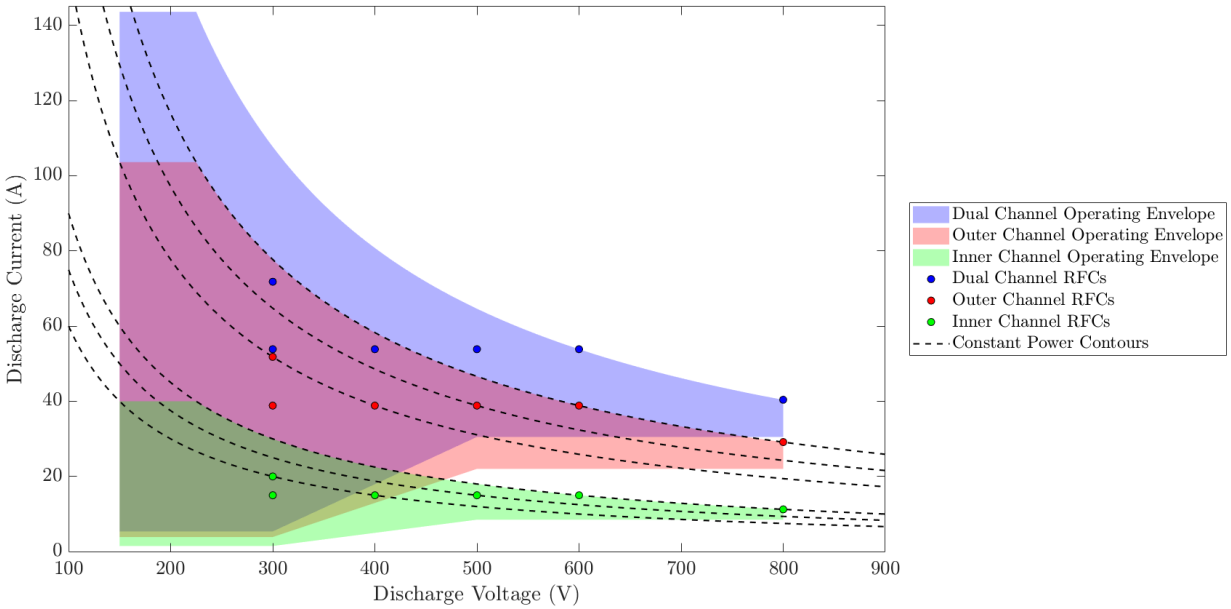

Fig. 5 A graphic representation of the full operational envelope of the thruster. The dots are the reference firing conditions for each firing configuration: inner channel only, outer channel only, and dual channel.

current of 144 A and voltage of 225 V. At 800 V, we expect the specific impulse to reach at least 2900 s. These predictions assume power can be added linearly when predicting dual channel operation despite knowing that the channels interact. One feature that is evident from the operating envelope is the overlap of achievable powers between different operating conditions. This feature, unique to nested Hall thrusters, allows for a larger range of thrust and specific impulse values for a given power depending on current mission needs. In other words, this graph depicts that high specific impulse performance is achievable over a much wider range of power levels (7 kW to 32 kW) than traditional Hall thrusters.

D. Component Features

1. Discharge Chamber

Similar to the H9, both discharge chambers (inner and outer) have a "U-shaped" wall and replaceable "rings" near the exit.[24] This design, originally from the H6, allows for easy integration of wall probes or a change of material to study plasma interactions.[37,47–49]

Figure 6 schematically shows this base and ring configuration. Nominally, both discharge chambers and all rings are made from a borosilicate ceramic. The inner discharge chamber shares the same mean diameter, length, and channel width as the H9. The outer discharge chamber shares the same length as the inner. The scaling for the mean diameter and the width for the outer channel was based on previous experience with the X2 and X3 as well as necessary spacing to fit the magnetic circuit.[14,15]

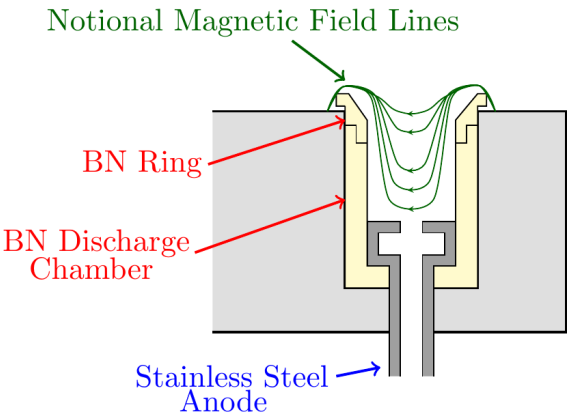

Fig. 6 A notional schematic of each discharge chamber for the NHT featuring an anode, a discharge chamber base and removable rings. Not to scale.

2. Anode/Gas Distributor

The combined anode and gas distributor is used to inject neutral propellant into the discharge chamber as well as provide the bias for the axial electric field. The anode for the inner channel, previously described[26,35], ensures high azimuthal uniformity of the neutral gas which is critical to efficient operation.

While the gas distributor geometry for the outer channel was scaled similarly to the scaling for the discharge chamber, the scaling of a few key parameters meant to achieve high flow uniformity, such as number of propellant inlets, were initially unknown. Thus, to ensure that the outer anode achieved similar performance to the inner anode, we performed numerical simulation on a variety of geometries. A three-dimensional simulation of xenon neutrals was performed using the computer code Monaco, an implementation of the direct simulation Monte Carlo method (DSMC).[50,51] The geometries considered were the entire anode geometry as well as the discharge chamber and rings. We used a diffuse wall condition at the thruster channel walls, and particles were allowed to escape the domain at the discharge chamber exit plane. The only location of inflow was at the anode inlet tubes. Simulated number density profiles were then extracted, in the same axial location as previous experimental anode flow uniformity tests to compare case to case.[24,25] Once a sufficiently uniform (criteria to be discussed in Section IV,A) was achieved with the simulation, the design for the outer anode was finalized.

3. Cathode

The cathode supplies electrons for both the discharge and neutralization of the plume. Here, we use a centrally-mounted lanthanum hexaboride (LaB_6) hollow cathode. This device is similar to the cathodes used for all the H6 and H9 testing.[25,33,34] The original component used for the H9 testing has been operated up to 60 A during development.[31,32] However, at its highest nominal operating condition, the N30 requires 71.8 amperes of current. Thus, a new cathode was required for this thruster. In order to achieve higher current, the LaB_6 insert size was increased to permit currents up to 100 A. However, the overall form factor of the cathode did not change. This was critical to enable this device to be used with both the H9 and N30 thrusters. Additionally, there are design features on the cathode that ensure the exit plane of the keeper is at the same axial location on both thrusters. During initial testing, the cathode was operated up to 60 A. This device is now the nominal electron source for both thrusters.

4. Magnetic Circuit

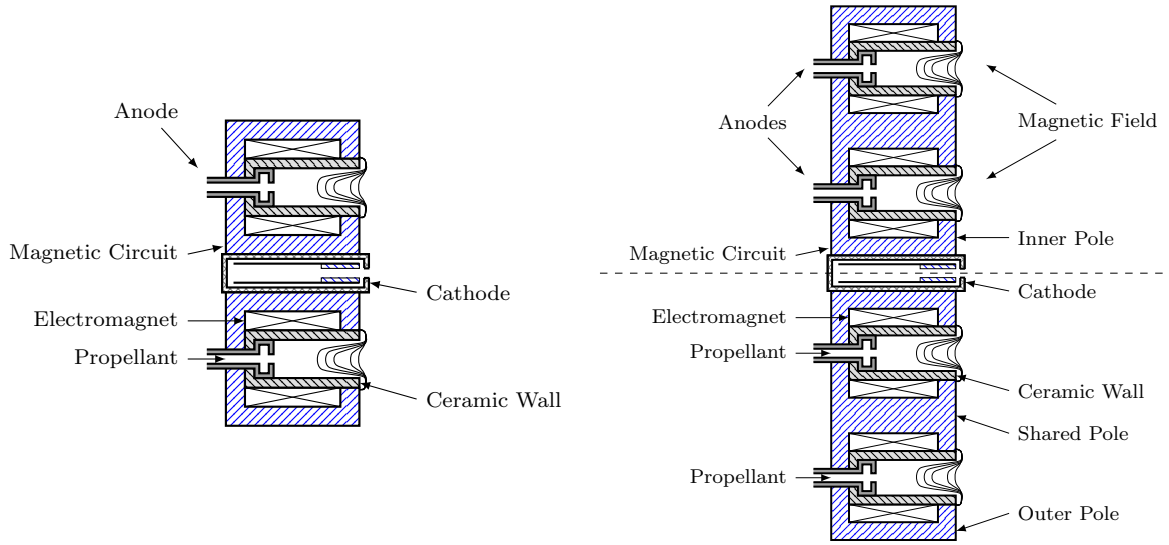

Fig. 7 A schematic detailing the differences between a standard Hall thruster (left) and a nested Hall thruster (right). Most notably, the nested Hall thruster has shared magnetics between each channel making magnetic field design challenging.

The magnetic field was numerically simulated using Infolytica's MagNetv7.7 software. A significant portion of the effort during the design phase was spent on the magnetic field, as the design of nested Hall thruster magnetic fields is inherently more complicated than single channel thrusters. This complexity is illustrated in Figure 7. When the thruster is operating in single channel mode (either the inner or outer), a NHT magnetic circuit acts similar to a standard Hall thruster. That is to say, the channel has two dedicated electromagnets and similar pole pieces. There still exists more physical magnetic material; however, the material from the other channel does not impact the field shape significantly. When running in dual channel mode, the outer magnetic poles for the inner channel also act as the inner magnetic poles for the outer channel. This shared pole makes the design of the magnetic circuit complicated as small changes impact both field shapes. Additionally, previous work showed that NHT magnetic fields are not simply the summation of single channel field and each firing condition must have its field optimized separately.[25]

Similar to the H9, the NHT does not use discrete outer coils. This ensures azimuthal uniformity of the magnetic field. In order to achieve the magnetic field shape and structure, we employ four electromagnets, two dedicated to each channel. These electromagnets allow us to vary the strength of the magnetic field and easily achieve 800 V operation of the thruster while remaining fully shielded. The saturation properties of the magnetic circuit for each channel are equal or better to those of the H9's circuit. While the starting geometry for the inner channel was that of the H9's, changes were made to the poles to ensure that the field in the discharge chamber was nearly identical to that of the H9's. The outer channel field has a similar shape, symmetry, and centerline profile as the inner channel. The downstream gradient of the field reduced in magnitude due to the widening of the channel as seen in Figure 8. Importantly, the depth of the grazing line is similar between the two channels.

Simulations by Mikellides et al. of the X3 showed that the difference in magnetic field gradient on channel centerline between the outer channel and the inner and middle channels led to changes in

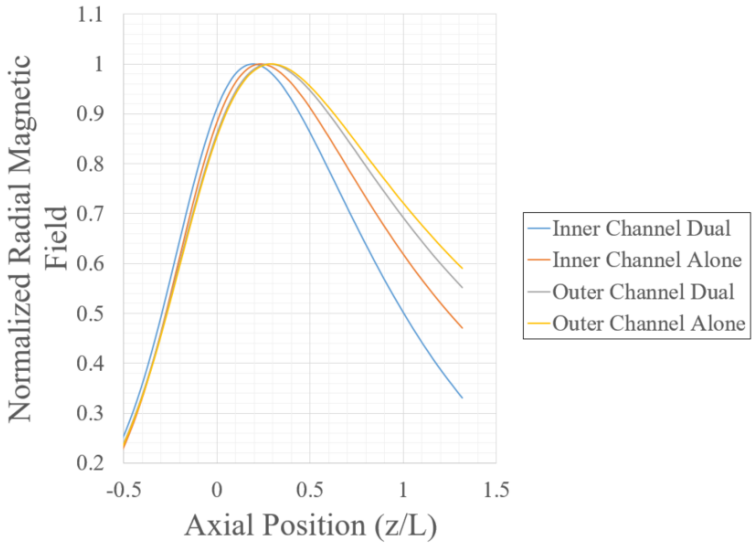

Fig. 8 Centerline profiles for all configurations of the magnetic field. The increase in the gradient for the inner channel alone versus in dual channel mode is evident.

downstream plasma potential.[42] They suggested that there was further room for magnetic field optimization because this change of gradient could impact the cathode coupling voltage and accelerating voltage for the channel. However, we found here that this change in magnetic field gradient difference of the peak is in fact inherent to the design of nested Hall thrusters. A simple dipole model shows that the presence of an outer magnetic field in fact "squeezes" the gradient on the inner channel. Thus, the inner channel gradient will always be greater than the outer channels in dual channel mode (as seen in Figure 8). This leads to the conclusion that it will always be challenging to get the same plasma potential downstream of the inner and outer channels. Additionally, cathode coupling will always be slightly different between the two channels.

The final and most critical part of the magnetic field design process was to optimize the field for all firing configurations. Previous worked showed that not optimizing the field for each firing configuration of an NHT could drive the plasma into the walls, leading to degrading performance and higher thruster oscillations.[17] Additionally, since magnetically shielded thrusters require the plasma to be "shielded" from the walls, non-optimized field could impact thruster lifetime. Thus, prior to manufacturing, simulations were performed to ensure that each firing configuration produced a shielded topology and to optimize the fields only changes to the electromagnet setpoints were necessary.

5. Other Features

While the component features listed above are most critical, there are several other important features of the thruster worth noting. First, many steps were taken to mitigate the high thermal load of the plasma and maintain reasonable temperatures for the thruster. These include the anodization of the thruster stand and a spray coating on the outer guide of the thruster. These processes both aim to increase the emissivity of their respective parts to enhance radiative heat transfer. Similarly, many parts of the magnetic circuit were "sand-blasted" to enhance their emissivity and encourage heat transfer to the outer surfaces of the thruster. In order to monitor the temperatures of the thruster, many thermocouples were integrated and embedded throughout to observe real-time thruster health.

The final two features of note are the pole covers and the thruster electrical configuration. Graphite pole covers were incorporated on the downstream surface of all poles. These pole covers prevent the erosion of the magnetic pole surfaces, which is known to be higher for magnetically shielded thrusters than unshielded thrusters.[52,53] Additionally, while there is the ability to run the thruster in any electrical configuration, the nominal configuration is "cathode-tied," where the body voltage is electrically-tied to cathode potential. This configuration limits the floating potential of the thruster to reduce pole erosion and extend lifetime.[43,54,55]

III. Test Equipment

In this section, we describe the facility and diagnostics used for acceptance testing and initial firing. We first detail the vacuum facility and then discuss the acceptance testing equipment, thrust stand, and probe system used.

A. Facility

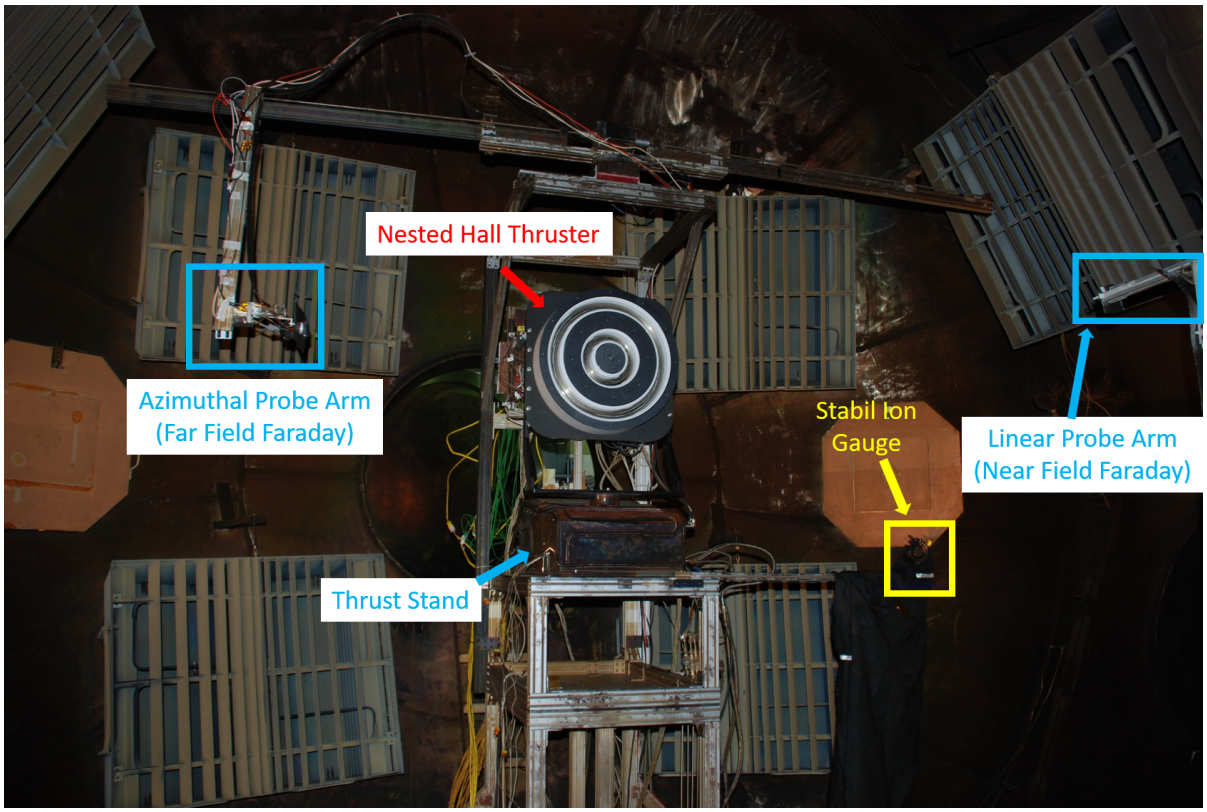

Fig. 9 A picture of the full setup inside the Large Vacuum Test Facility for initial firing

All testing (including anode flow testing) occurred in the Large Vacuum Test Facility at the University of Michigan. The facility, which is six meters in diameter and nine meters long, uses four mechanical pumps to achieve rough vacuum. The chamber has thirteen LN_2-baffled TM-1200 CVI cryopumps and six copper cryogenic "thumpers" in order to achieve high vacuum. Typically, eighteen of the nineteen pumps were used during operation. Pressure was monitored using a Series 370 Stabil Ion gauge. The chamber was outfitted with two gauges: one on the wall of the facility and one mounted roughly 1 meter from the thruster in line with the exit plane. The latter gauge had a grounded copper mesh surrounding the entrance to prevent ambient plasma from entering. All pressures reported are from

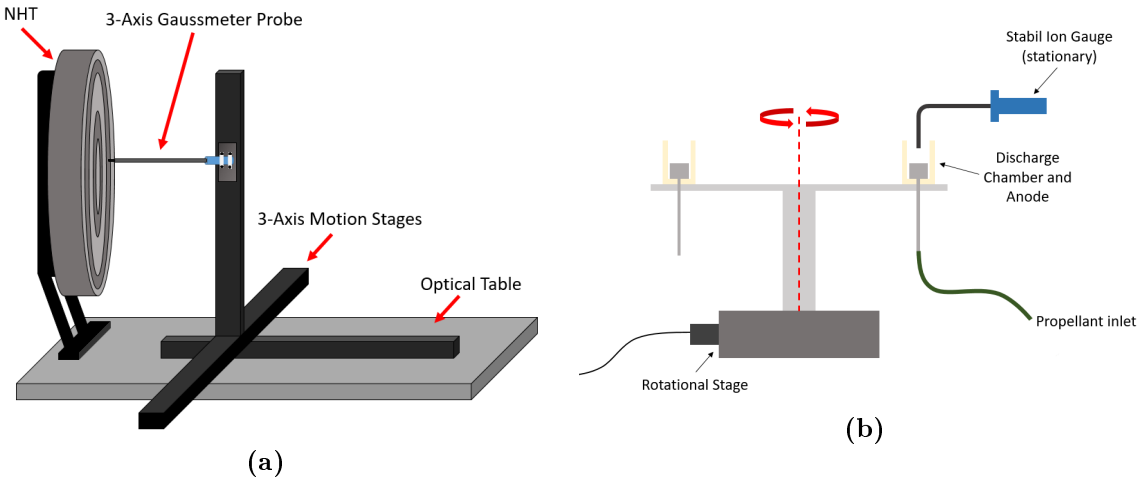

Fig. 10 Schematic of the setup for both (a) the magnetic field mapping and (b) the anode flow uniformity testing.

the latter per industry standard.[56] Base pressures were below 0.1 μTorr-Xe and typical operational pressures varied from 4 to 16 μTorr-Xe.

While nested Hall thrusters can be run off a single power supply, we used an independent commercially-available power supply for each channel. The inner and outer channel power supplies have a maximum output power of 60-kW and 150-kW respectively. The negative side of the power supplies (cathode return) were shorted together at the power feedthrough into the chamber. Power for the four electromagnets, heater, and keeper was supplied from external, commercially-available rack-mounted supplies. Three commercially-available flow controllers were used to supply aerospace propulsion grade xenon to the cathode, inner anode, and outer anode.

B. Diagnostics

1. Acceptance Testing

In order to verify that both the magnetic circuit was properly constructed and that the field matched our simulations, we mapped the thruster's magnetic field with a 3-axis Gaussmeter and compared the measurements to the simulations. A schematic of the setup can be seen in Figure 10a. We took two-dimensional (r-z) maps. Additionally, we measured the maximum centerline radial magnetic field to assess saturation of the circuit. Finally, we performed all these studies in all three magnetic field configurations. In order to pass acceptance testing, we establish the follow criteria: a qualitative agreement of the two-dimensional maps of simulated versus measured fields and a 25% margin on the nominal magnetic field for saturation onset (greater than 5% deviation from linearity).

The second major acceptance test performed was the anode flow uniformity test. The setup for this test can be seen in Figure 10b. Azimuthal flow uniformity was assessed by neutral density testing with a Series 370 Stabil Ion Gauge. The discharge chamber, BN rings and anode were placed on a rotational stage with the ion gauge inlet located radially on channel centerline and axially midway through the discharge chamber.[26] Each anode (inner and outer) were measured at 36 evenly distributed azimuthal points. For the inner channel, we performed these tests at 2 mg/s and 20 mg/s. For the outer channel, we performed these tests at 5 mg/s and 50 mg/s. The dwell time at each

test point was 10 seconds. For the inner anode, an acceptable flow uniformity criterion of deviations up to 10% (δp_{max}) from the mean value ($\langle p \rangle$) was used during testing.[57] For the outer anode, while the same criterion is desired, this would be particularly challenging at the lower flow rate since the internal volume of the anode is significantly larger. The X3 Hall thruster used deviations of up to 24% from the mean value for the large anodes.[40] The middle anode of that thruster exhibited fluctuations of 14.7%.[40] Based on this, we relax our criterion from the inner anode to be 20% of the mean value for the low flow case while maintaining a criterion of 10% for the high flow case.

2. Standard Telemetry

Standard telemetry (DC values) was recorded using LVTF's data acquisition system which is LabView based, optically isolated, and logs data every 1 second. These values include electromagnet, heater, keeper, discharge, and body currents and voltages, facility pressure, anode and cathode flow rates, and cryo and thruster temperatures. Additionally, high-speed thruster oscillations were measured using Tektronix AC coupled clamp-on current probes and Tektronix high-speed differential voltage probes. We then recorded the anode current oscillations, cathode current oscillation, discharge voltage oscillations, and cathode-ground voltage oscillations using a four-channel 500 MHz, 5 MSa/s per channel Agilent oscilloscope.

3. Thrust Stand

We measured the thrust produced using an inverted pendulum thrust stand.[58,59] A picture of the thruster on the thrust stand is shown in Figure 10. The thrust stand was water cooled to maintain a constant power. The thrust stand operated in null mode with active inclination control. The displacement was measured using an optical sensor. The thruster was run through an outgassing and warm up procedure before any measurements were taken. Calibrations were performed by dropping a series of known mass weights; inclination was controlled during calibration. An inclination calibration was also performed and inclination drift was accounted for in post-processing.

In order to accommodate the higher-than-average mass of the thruster, a number of changes were made to the thrust stand. Here, the "nominal" thrust stand condition is that of the H9. Most notably, the spring used as a restoring force was changed to a stiffer spring and the flexures were changed to torsional bearings that can support higher masses. Both of these changes had previously been done for testing the X3.[18] Nonetheless, in order to ensure that the thrust stand was still reporting reliable thrust values, we validated this new configuration by testing the H9 on the stand. To get reasonable response, we also added "dummy" masses to the stand to simulate the higher mass of the NHT. We tested the H9 at two of its nominal conditions (300 V, 15 A and 600 V, 15 A). The results showed the thrust measured was well within uncertainty as compared to the nominal configuration. The measured uncertainty for the thrust stand was 3%.

4. Probes

To assess plume symmetry, we used a far-field Faraday probe. The probe had a collector diameter of 6.1 mm and was swept azimuthally from 0 to 180 degrees. To ensure ion saturation, the collector and guard ring were biased to -20 V. Current was measured using a Keithley Series 2400 Sourcemeter.

IV. Acceptance Testing

In this section, we first present the results from the anode flow uniformity testing and then the results from the magnetic field mapping.

A. Anode Flow Uniformity

Figure 11 shows the results of the anode flow uniformity testing. The facility pressure during this testing was between 1 and 10 μTorr-Xe. The inner anode is well within acceptable limits with the largest deviations at low flow being 4.6% and at high flow being 4.0%. For the outer anode, the largest deviations were 15.3% at low flow and 8.4% at high flow. The low flow condition saw higher deviations from the mean than high flow, however this is expected and the outer anode is never expected to run at 5 mg/s. Regardless, all conditions met the acceptance criteria and thus we determined that both anodes passed flow uniformity testing.

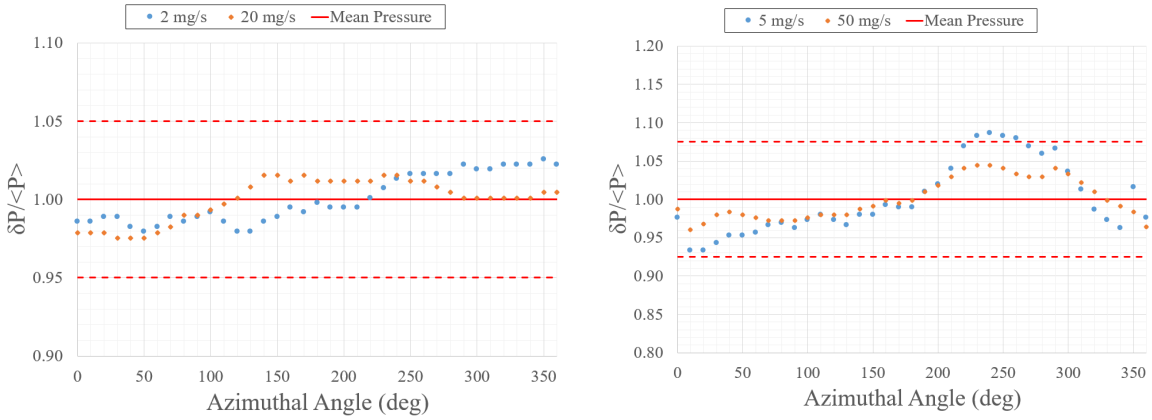

(a) Inner Anode **(b) Outer Anode**

Fig. 11 Results of the anode flow uniformity testing for both anodes.

B. Magnetic Field Testing

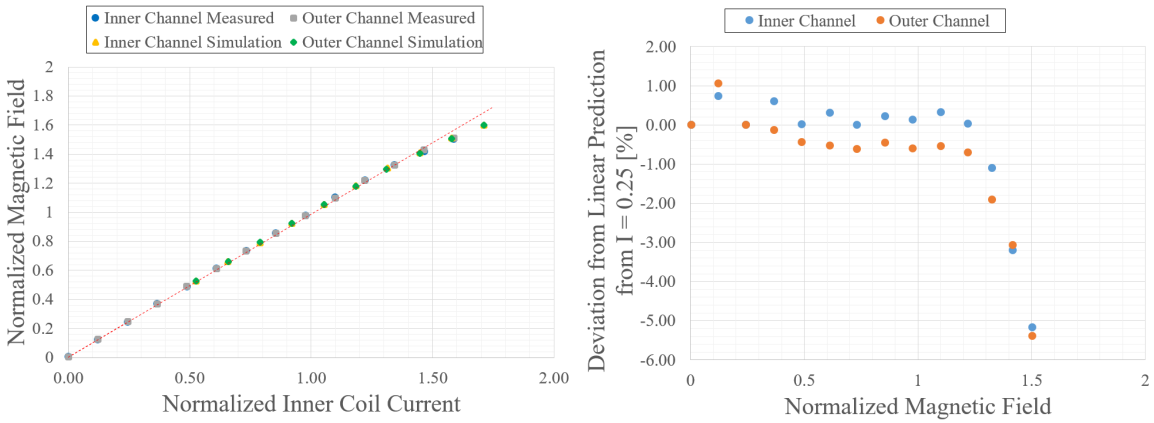

(a) **(b)**

Fig. 12 Saturation Profile for the Dual Channel Magnetic Field

Overall, the two-dimensional mapping revealed that each thruster configuration matched the simulation very well. Figure 12a shows the response of the magnetic circuit with increasing inner coil current with a constant coil ratio. In order to facilitate ease of comparison between cases, the inner coil current has been normalized. Note that only simulation data above normalized current of 0.5 is presented. Overall, the results indicate that the circuit is linear up to magnetic fields 50% higher

than nominal strengths. This allows for a margin on the strength and expanded research capabilities. Figure 12b shows this more clearly by plotting the departure from linearity versus magnetic field. In order to generate this plot, we predict the strength for a given coil current based on the strength at a normalized inner current of 0.25 (using a ratio). We then compared the predicted value to the actual measured value. This departure does not go above 5% until the normalized magnetic field is above 1.5. It is also critical to note that Figure 12a demonstrates very close agreement with the simulation, particularly in the saturation region. At many of the points, the simulation and experimental data are indistinguishable.

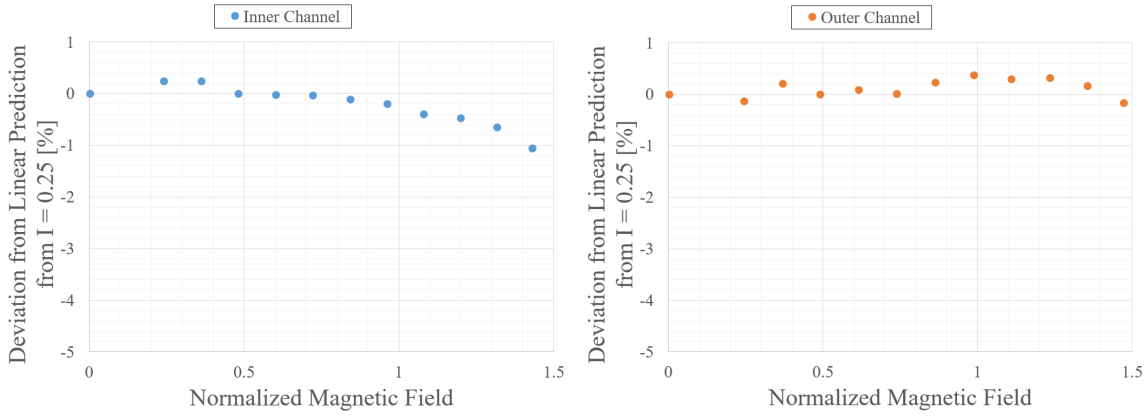

(a) **(b)**

Fig. 13 Saturation profiles for the inner channel only magnetic field (a) and outer channel only magnetic field (b).

Similarly, Figure 13 indicates the deviations from linearity for the single channel configurations. These results show that the single channel configurations show less saturation as compared to the dual channel field. This indicates that these fields actually have greater margin than in dual channel mode. This is likely due to less magnetic flux being pushed through the material in single channel mode. Given these results and qualitative observations of the two-dimensional mapping, we ultimately determined that all three thruster configurations pass acceptance testing.

V. Performance Testing

In this section, we present the initial performance testing of the thruster including evidence of magnetic shielding, current density, oscillation and thrust measurements. Unanticipated challenges in the implementation of a continuous monolithic piece of borosilicate ceramic for the outer channel discharge chamber precluded most outer channel and all dual channel measurements in this initial campaign (discussed more in Sec. VI). Therefore, we only report inner channel performance.

A picture of the thruster, during first lighting, is shown in Figure 14. We see both the inner and outer channels running alone here. Qualitatively, the plumes look characteristic of typical Hall thruster plumes.

A. Magnetic Shielding

Throughout the test campaign, there were many qualitative indications that the channels were magnetically shielded. Typical qualitative indications of magnetic shielding include low luminosity near

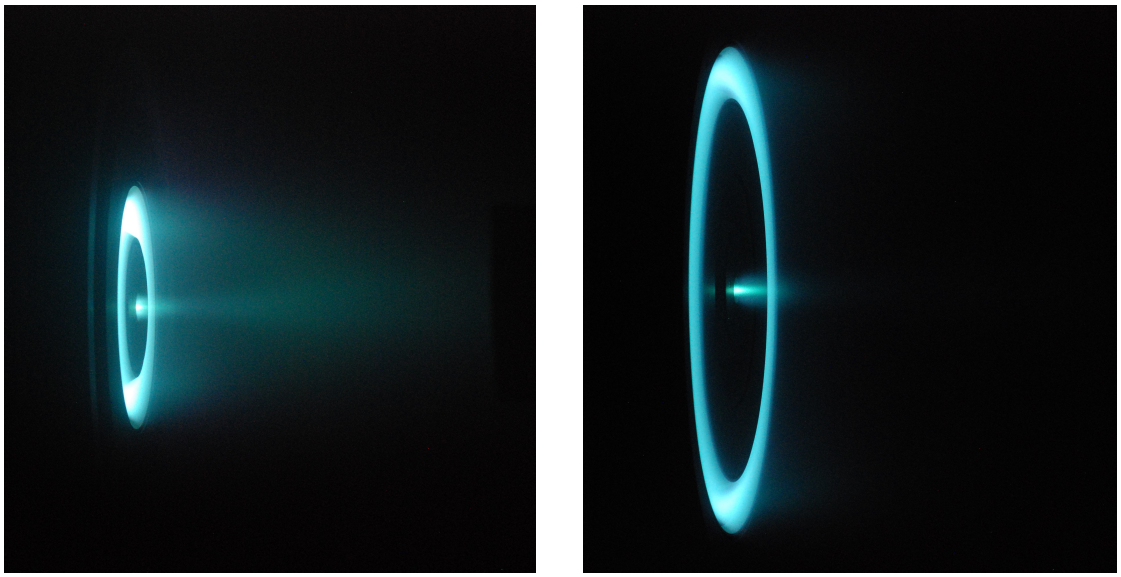

(a) (b)

Fig. 14 A picture of the inner channel running alone at 300 V, 15 A (a) and the outer channel running alone at 300 V, 38.85 A (b). Note, the camera settings are not the same between these two photographs.

the walls and carbon build-up on the walls.[24,60] For an unshielded thruster, there is high luminescence radially throughout the discharge chamber. However, with a magnetically shielded thruster, a low electron temperature is expected near the wall because the grazing line samples low temperature plasma near the anode and magnetic field lines are approximately isothermal. This low electron temperature then leads to low luminescence. This feature can been seen on the inner channel in Figure 15a.

Additionally, for unshielded thrusters, we expect to see carbon deposition (from the downstream beam dump) deep into the discharge chamber. Closer to the exit plane however, the rings should remain white from erosion. For shielded thrusters, the walls would remain coated even near the exit plane. Figure 15b shows a picture of the inner channel after approximately 50 hours of firing. We see that the entirety of the discharge chamber (both inner and outer walls) is coated in carbon, again suggesting that the thruster is magnetically shielded. Additionally, chamfer laser induced fluorescence measurements confirming magnetic shielding were taken and will be published in the near future. We note that these observations alone are not sufficient to claim the thruster is shielded. However, these indications, in combination with the heritage from the H9 and H6MS, give us confidence to say that it is shielded. Finally, while we are unable to assess the shielding of dual channel mode, we are confident that this configuration will also be magnetically shielded based on the magnetic field mapping, heritage, and the indications given in single channel mode.

B. Oscillations

We characterized the plasma oscillations of each channel. Table 2 shows the anode current peak-to-peak, discharge voltage peak-to-peak, and the first and second peak frequencies (highest and second highest amplitude) of the power spectrum for each reference firing condition for the inner channel. The peak magnetic field strength was the same for each condition and the same as the H9. Interest-

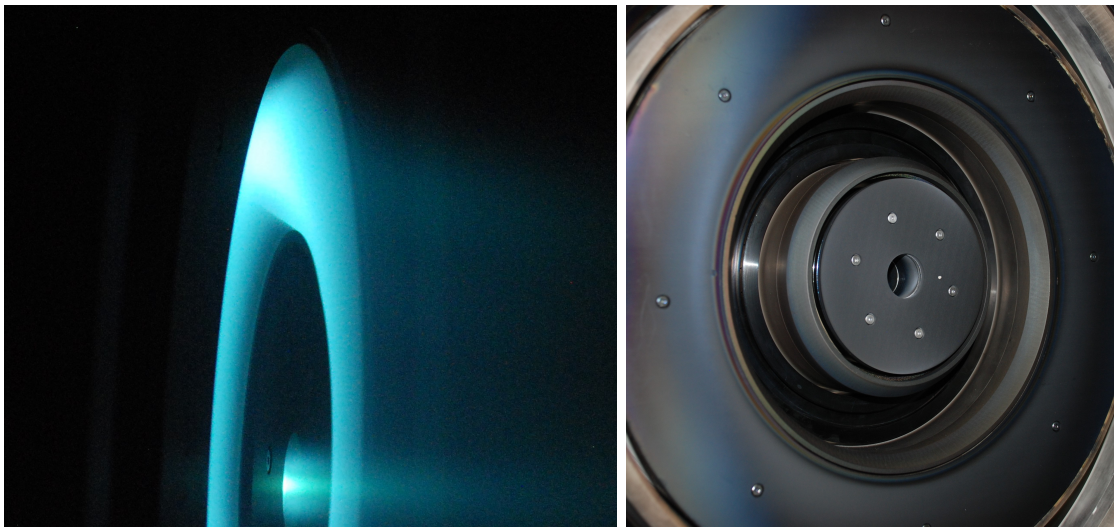

(a) (b)

Fig. 15 A picture of the inner channel running (a) where a region of high light emission can be seen at the center of the channel; near the walls, there is significantly lower light emission. A picture of the inner channel (b) after approximately 50 hours of firing showing carbon buildup over the entire wall.

Table 2 Plasma Oscillations for the Inner Channel Reference Firing Conditions

Voltage (V)	Current (A)	Current P2P (A)	I_{P2P}/I_d (%)	Voltage P2P (V)	V_{P2P}/V_d (%)	1^{st} Peak Freq. (kHz)	2^{nd} Peak Freq. (kHz)
300	15	5.2	34.8	23	7.7	43.9	8.4
300	20	6.8	34	27	9	9.3	46.2
400	15	12.5	83.4	48	12	24.8	9.8
500	15	12.5	84.5	55	11	63.1	14.8
600	15	12.1	81.3	53	8.8	66.4	10.8
800	11.25	8.8	78.2	68	8.5	77.6	14.0

ingly, the peak frequency for each condition is higher than a typical Hall thruster breathing mode. We believe this frequency to be associated with the cathode.[61,62] It is possible that these cathode oscillations are stronger than the original H9 measurements because the cathode used is a new cathode with a higher nominal current and flow rate. Thus, at lower currents and flow rates, the cathode oscillations increase.[33] By comparison, the cathode oscillations did not dominate the H9 until 500 V. Based on this evidence, we believe the breathing frequency to be the frequency of the second highest amplitude. These frequencies are similar to the H9 breathing frequencies (between 9 and 18 kHz).[24]

Figure 16 shows the power spectrum of these oscillations in which the cathode oscillation and breathing frequency are evident. Similar to the H9, there still exists a clear transition at about 500 V where the cathode oscillations become more peaked. Oscillation data from the outer channel (300-500 V) showed no prominent cathode peak until 500 V; however, the breathing frequency was much higher (19-35 kHz). This emergence of the cathode peak at higher voltages is similar to the behavior of the

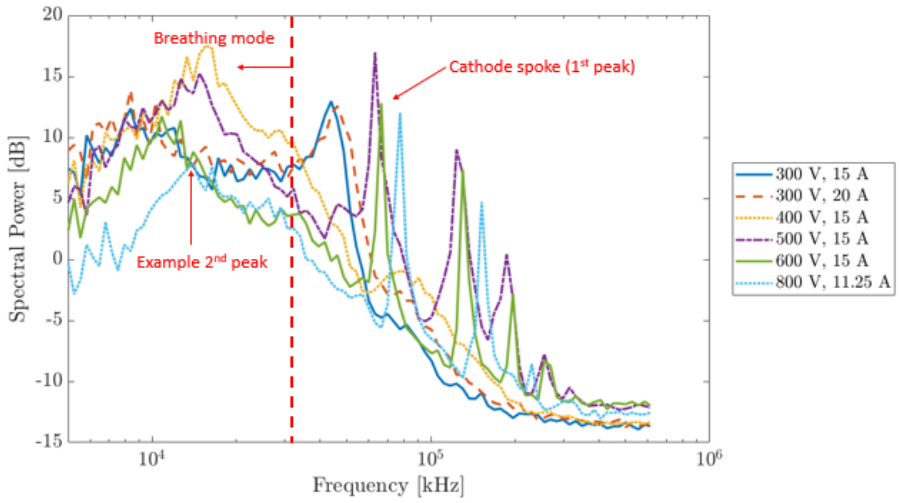

Fig. 16 Power spectrum of the discharge (anode) current oscillations for all reference firing conditions for the inner channel.

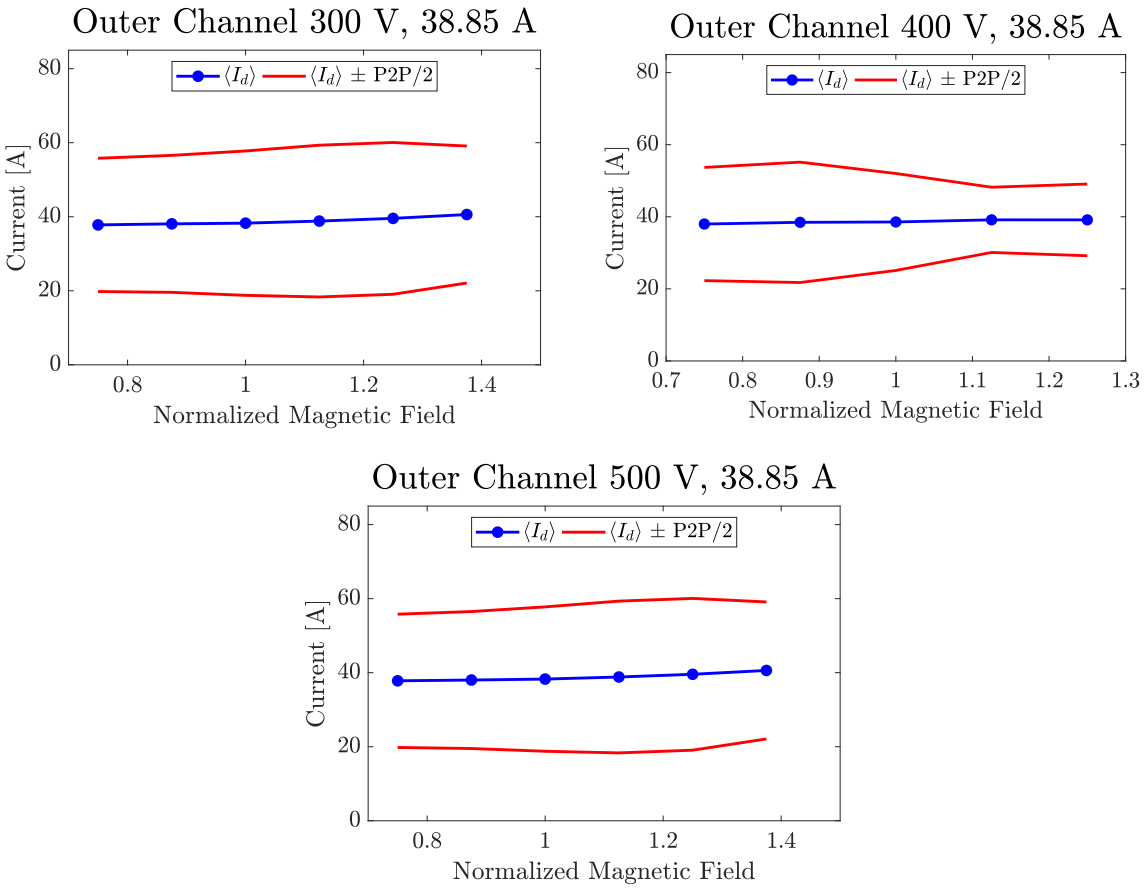

Fig. 17 Magnetic field sweeps for a selection reference firing condition for the outer channel. The plots show mean discharge current and peak-to-peak for varying magnetic field strength.

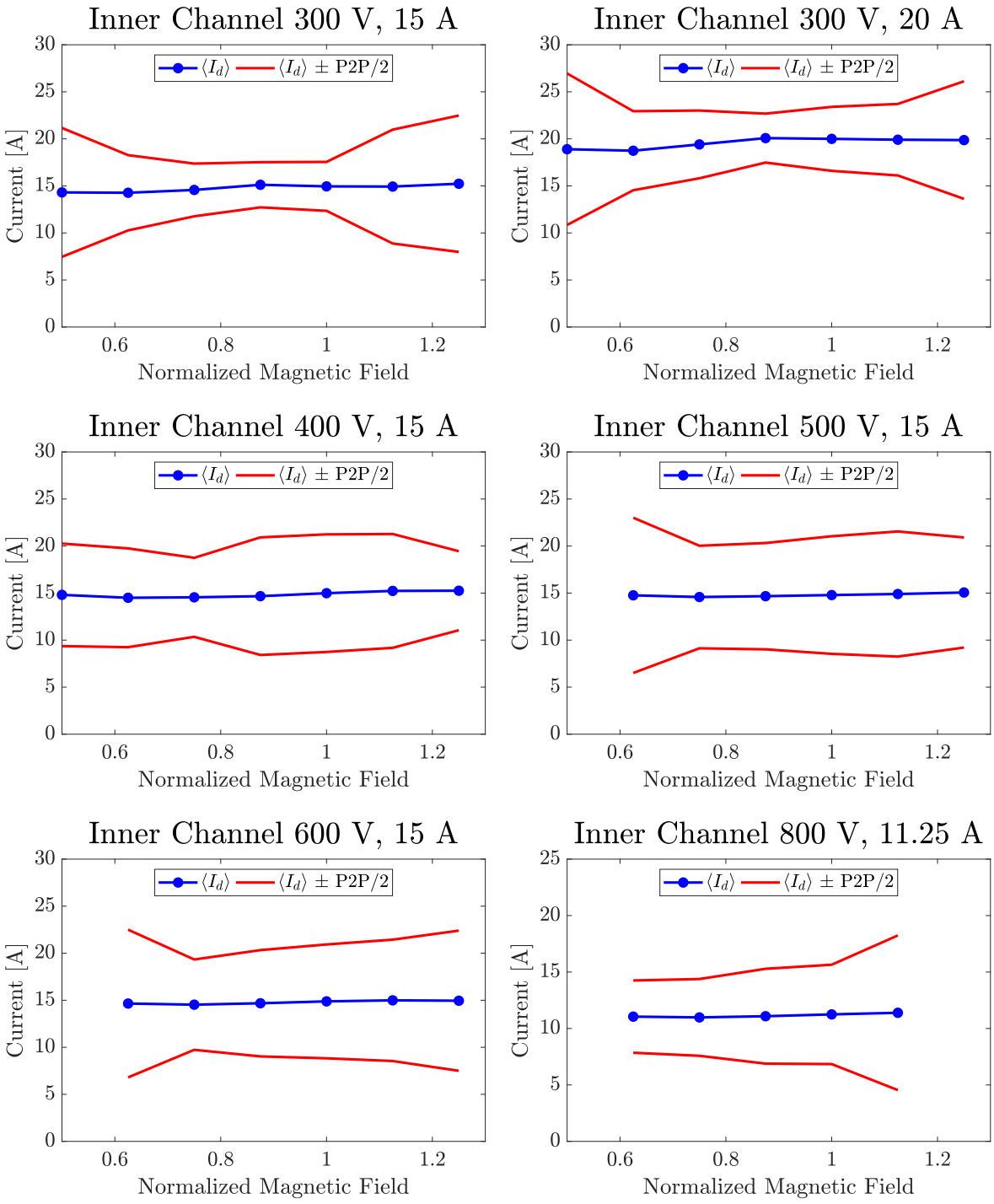

Fig. 18 Magnetic field sweeps for each reference firing condition for the inner channel. The plots show mean discharge current and peak-to-peak for varying magnetic field strength.

H9. The lack of cathode oscillations at low voltage is likely due to the much higher flow rates through the cathode (2.7x at 300 V), which have been shown to damp oscillations.[33]

Finally, Figures 17 and 18 plot the mean current and peak-to-peak oscillations for the firing conditions presented here. Overall, we see that the N30 is stable over the RFCs with the highest peak-to-peak amplitude at 101% of the mean current. The dominant frequencies are typical of magnetically shielded Hall thrusters.[24,61,62] The magnetic field sweeps also show a wide range of magnetic stability margin.[43]

C. Performance

Once the "nominal" magnetic field had been determine, we performed thrust measurements at each of the RFCs for the inner channel. Table 3 shows the results from this study. Telemetry shows that the cathode-ground voltage varied from -10.6 to -12.1 V and the body current varied from -0.56 to -1.73 A. The negative sign indicates electron current is collected on the body . Overall, the thrust, efficiency, and specific impulse are in line with other state-of-the-art magnetically shielded thrusters.[21,24,25,43] The thrust ranges from 292.1 to 450.6 mN with a peak specific impulse of 2831 seconds at 800 V discharge voltage and a peak efficiency of 65.2% at 600 V.

Table 3 Thrust and Performance Metrics for the Inner Channel at all RFCs

V_d (V)	I_d (A)	P_d (kW)	Anode (mg/s)	Cathode (mg/s)	$\frac{P_{mag}}{P_d}$	Thrust (mN)	Total I_{sp} (s)	Total Eff	Pressure (μTorr-Xe)
300	15	4500	14.70	1.03	1.60%	292.1	1893	0.593	5.1
300	20	6000	18.30	1.28	1.20%	376.6	1960	0.596	6.3
400	15	6000	15.26	1.07	1.19%	351.2	2189	0.619	5.3
500	15	7500	15.91	1.11	0.94%	406.4	2434	0.641	5.5
600	15	9000	16.00	1.12	0.78%	450.6	2680	0.652	5.6
800	11.25	9000	13.18	0.98	0.82%	392.9	2831	0.603	4.7

D. Ion Current Density

Figure 19 shows the far-field ion current density traces for both the inner and outer channels. Qualitatively, for both channels, we see evidence of plume symmetry at each operating point. There are some slight differences (imperceptible) in the height of the two peaks for each case, which can be attributed to variations in neutral density azimuthally as shown in anode flow uniformity measurements. However, the difference in peak height is less than 10% for all traces taken (all six conditions for the inner channel and the three cases presented for the outer channel). These traces indicate that each channel performs as expected across the nominal operating envelope.

VI. Discussion

One the key goals of the N30 was to create a nested Hall thruster where the inner channel is geometrically the same as the H9. Thus, we would have the ability to make direct comparisons between the performance of the inner channel in the thruster is various modes with the H9. As a baseline, we compare the inner channel operating alone and the H9. The differences between these two configu-

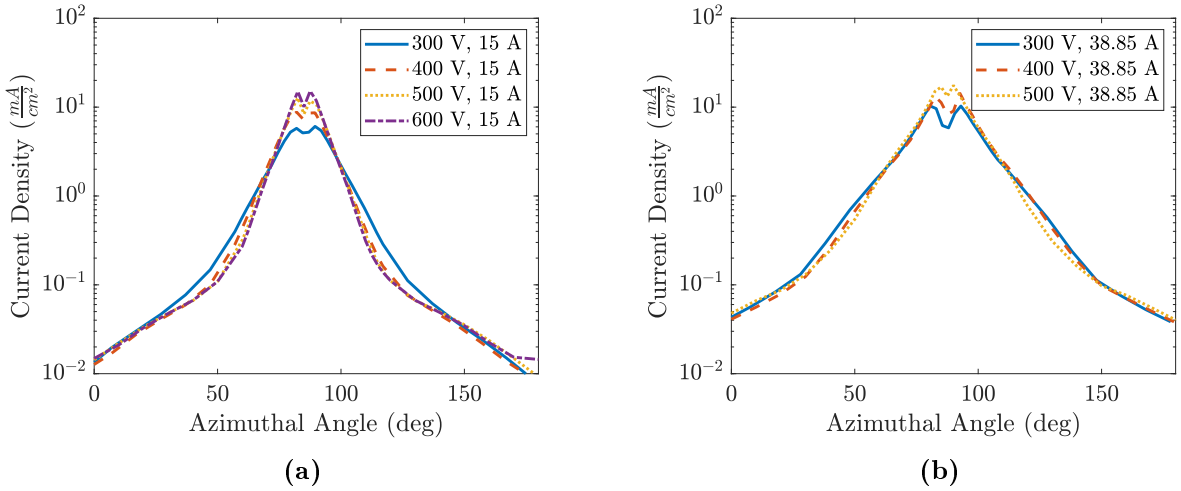

Fig. 19 Ion current density measurements with increasing voltage for the inner channel (a) and outer channel (b) at constant current.

rations are the amount of magnetic material present, the thermal environment, and subtle changes to the magnetic field shape in the far-field. The peak magnetic field magnitude was the same. The results of this comparison are seen in Table 4. The 800 V condition is not presented because data for the H9 at the same settings is not available. Overall, we see that the H9 and the inner channel of the NHT have very similar performance. Almost all values are within their uncertainties. This result indicates two key findings: (1) we were able to reproduce the H9 as the inner channel of an NHT and (2) running a thruster in a different thermal and magnetic material environment does not have drastic impacts on the performance.

Table 4 Comparison of the inner channel of the N30 and the H9 at five RFCs. Standard error for the NHT results was 3%.

	Thrust (mN)			Total I_{sp} (s)			Total Efficiency		
Condition	H9	NHT	% Diff	H9	NHT	% Diff	H9	NHT	% Diff
300V, 15A	286.8	292.1	1.8%	1914	1893	-1.1%	0.598	0.593	-0.8%
300V, 20A	371.8	376.6	1.3%	1987	1960	-1.4%	0.603	0.596	-1.1%
400V, 15A	345.1	351.2	1.8%	2196	2189	-0.3%	0.619	0.619	0.1%
500V, 15A	392.8	406.4	3.5%	2422	2434	0.5%	0.622	0.641	3.0%
600V, 15A	435.6	450.6	3.4%	2652	2680	1.0%	0.629	0.652	3.5%

While there are no drastic differences between the H9 and the NHT inner channel, there are a few key variations to note. The body current collected is notably higher for the NHT than the H9. This is not surprising as the NHT has a much larger area to collect body current over due to the presence of another channel. Additionally, the mass flow rates (2-3%) and thrust (1.3-3.5%) were slightly higher for the NHT than the H9. Regardless, the performance differences are on the order of the uncertainty of the measurements. That is why, despite having slightly higher thrust for all conditions, the specific impulse and efficiency see both increase and decreases between the two thrusters. However, it is important to note that the NHT inner channel studies occurred at 60-70% lower pressures than the

H9 due to differences in pumping speed between the two tests. Based on H6MS results, changes in pressure should not lead to large changes in thrust; however, it can have a more noticeable impact on total flow. Therefore, at equal pressures, the flow rates would likely be the same[63] Should this be true, when operating at the same pressures, there may exist a 2-3% increase in specific impulse and efficiency for the inner channel of the NHT as compared to the H9 across the board. This is likely due to the thermal differences, where the NHT was, on average, operating at approximately 200 °C less than the H9. Additionally, subtle changes in the far-field magnetic field could impact the location of the acceleration region and the cathode coupling. Movement of the acceleration region, with pressure, could account for differences in mass flow rates as well.

The N30 is a significant step for nested Hall thruster technology, and we showed here state-of-the-art performance and magnetic shielding. However, there do remain some key challenges. First and foremost, we have yet to run this thruster up to full power. Based on heritage arguments and some basic thermal calculations, we believe the thruster will be thermally stable over its entire operating range. However, it is challenging to know whether we will encounter thermal issues at 33 kW until we test at this condition. While we took measured steps to improve the thermal environment, the compactness of the thruster will always make thermal stability a difficult endeavor. Finally, a large area for improvement lies in discharge chamber materials. As mentioned earlier, challenges with the discharge chamber precluded most testing with the outer channel. Likely, this was due to thermal expansion mismatches and tolerance-ing of the machined parts. For much larger parts (such as this discharge chamber compared to the inner), small issues with either of these can have much larger consequences due to accumulated errors on large diameters. We believe moving away from a single monolithic piece of ceramic would be advantageous. Due to advances in magnetic field topologies, graphite discharge chamber walls are now feasible.[37] Applying these new materials and designs to large channels in nested Hall thrusters is critical for future next generation missions from a cost and manufacturing perspective.

The main goals of the N30 were to design and implement a nested-channel thruster with a magnetic shielding topology, capable of 25-50 kW of discharge power. Additionally, we wanted the inner channel to share geometry with the H9 to enable channel interaction studies, to provide a NHT testbed, and to make the design modular for ease of diagnostic and mechanical changes. Considering the work presented here, we believe all of these goals have been accomplished. Indeed, all expect the discharge power capabilities have been demonstrated and considering the power levels each individual channel has been capable of, there exist no indications that this last goal has not been achieved.

VII. Conclusion

We presented here the design, fabrication, assembly and initial testing of the N30 dual channel magnetically shielded thruster. This thruster represents the first nested Hall thruster with the magnetic shielding topology. Notably, the inner channel of this thruster has the same geometry and similar magnetic field as the H9, allowing for a better understanding of nested Hall thrusters moving forward. The anodes passed initial acceptance testing with maximum anode flow uniformity deviations ranging from 4.0-8.4% at the high flow condition. The magnetic circuit passed magnetic field mapping, showing at least 50% margin on the nominal magnetic field setting. Saturation of the magnetic circuit was accurately predicted by the model. Characterization shows the inner channel reaching peak efficiencies of 65% and peak specific impulses of 2831 seconds which is within 4% of the H9 thruster. We successfully demonstrated magnetic shielding of the inner channel up to 800 V. The thruster showed a wide range of stability over magnetic field strengths for both the inner and outer channel.

Faraday probe measurements showed plume symmetry within 10% peak height. Characterization of the outer channel and dual channel configurations is ongoing. Indications are that the NHT is performing similar to other state-of-the-art magnetically shielded Hall thrusters. provides preliminary evidence that shielding can be achieved in a. nested geometry. On-going work is being performed for outer channel and dual channel operation. This moderate power device will serve as a laboratory testbed for addressing outstanding questions related to technology development, feasibility, and channel interactions in nested Hall thrusters.

Acknowledgments

The authors would like to acknowledge funding provided by the NASA Space Technology Research Fellowship grant numbers NNX15AQ43H and NNX15AQ37H, and National Defense Science and Engineering Graduate (NDSEG) Fellowship, sponsored by the Air Force Research Laboratory (AFRL). The authors would also like to thank Ray Swindlehurst at JPL for all his help during thruster design as well as the members of the Plasmadynamics and Electric Propulsion Laboratory for all their support during fabrication and initial testing. Portions of the research described in this paper were carried out at the Jet Propulsion Laboratory, California Institute of Technology, under a contract with the National Aeronautics and Space Administration.

References

[1] Herman, D. A., Tofil, T. A., Santiago, W., Kamhawi, H., Polk, J. E., Snyder, J. S., Hofer, R. R., Picha, F. Q., Jackson, J., and Allen, M., "Overview of the Development and Mission Application of the Advanced Electric Propulsion System (AEPS)," 2018.

[2] Crusan, J. C., Smith, R. M., Craig, D. A., Caram, J. M., Guidi, J., Gates, M., Krezel, J. M., and Herrmann, N. B., "Deep space gateway concept: Extending human presence into cislunar space," *2018 IEEE Aerospace Conference*, IEEE, 2018, pp. 1–10.

[3] McGuire, M. L., Burke, L. M., McCarty, S. L., Hack, K. J., Whitley, R. J., Davis, D. C., and Ocampo, C., "Low thrust cis-lunar transfers using a 40 kW-class solar electric propulsion spacecraft," 2017.

[4] Frisbee, R. and Hoffman, N., "Electric propulsion options for Mars cargo missions," *32nd Joint Propulsion Conference and Exhibit*, 1996, p. 3173.

[5] Andrews, D. and Wetzel, E., "Solar Electric Space Tug to Support Moon and Mars Exploration Missions," *Space 2005*, 2005, p. 6739.

[6] Manzella, D. H. and Hack, K., "High-power Solar electric propulsion for future NASA missions," *50th AIAA/ASME/SAE/ASEE Joint Propulsion Conference*, 2014, p. 3718.

[7] Strange, N., Merrill, R., Landau, D., Drake, B., Brophy, J., and Hofer, R., "Human missions to Phobos and Deimos using combined chemical and solar electric propulsion," *47th AIAA/ASME/SAE/ASEE Joint Propulsion Conference & Exhibit*, 2011, p. 5663.

[8] Brophy, J., Gershman, R., Strange, N., Landau, D., Merrill, R., and Kerslake, T., "300-kW solar electric propulsion system configuration for human exploration of near-earth asteroids," *47th AIAA/ASME/SAE/ASEE Joint Propulsion Conference & Exhibit*, 2011, p. 5514.

[9] Díaz, F. C., Carr, J., Johnson, L., Johnson, W., Genta, G., and Maffione, P. F., "Solar electric propulsion for human Mars missions," *Acta Astronautica*, Vol. 160, 2019, pp. 183–194.

[10] Jackson, J., Allen, M., Myers, R., Hoskins, A., Soendker, E., Welander, B., Tolentino, A., Hablitzel, S., Hall, S., Gallimore, A., et al., "100 kW Nested Hall Thruster System Development," 2017.

[11] Chang Diaz, F., Squire, J. P., Carter, M., Corrigan, A., Dean, L., Farrias, J., Giambusso, M., McCaskill, G., and Yao, T., "An Overview of the VASIMR® Engine," *2018 Joint Propulsion Conference*, 2018, p. 4416.

[12] Slough, J., Kirtley, D., and Weber, T., "Pulsed plasmoid propulsion: The ELF thruster," *31th International Electric Propulsion Conference*, 2009, pp. 20–24.

[13] Hall, S. J., Jorns, B., Gallimore, A., and Hofer, R. R., "Expanded thruster mass model incorporating nested Hall thrusters," *53rd AIAA/SAE/ASEE Joint Propulsion Conference*, 2017, p. 4729.

[14] Liang, R., *The Combination of Two Concentric Discharge Channels into a Nested Hall-Effect Thruster*, Ph.D. thesis, University of Michigan, 2013.

[15] Florenz, R., *The X3 100-kW Class Nested-Channel Hall Thruster: Motivation, Implementation, and Initial Performance*, Ph.D. thesis, University of Michigan, 2014.

[16] Cusson, S., Georgin, M., Dragnea, H., Dale, E., Dhaliwal, V., Boyd, I., and Gallimore, A., "On channel interactions in nested Hall thrusters," *Journal of Applied Physics*, Vol. 123, No. 13, 2018, pp. 133303.

[17] Cusson, S., Hall, S., Hofer, R., Jorns, B., and Gallimore, A., "The Impact of Magnetic Field Coupling Between Channels in a Nested Hall Thruster," *Proceedings of the 35th International Electric Propulsion Conference, Atlanta, Georgia*, 2017.

[18] Hall, S. J., Jorns, B. A., Gallimore, A. D., Kamhawi, H., Haag, T. W., Mackey, J. A., Gilland, J. H., Peterson, P., and Baird, M. J., "High-power performance of a 100-kW class nested Hall thruster," *Proceedings of the 35th International Electric Propulsion Conference, Atlanta, Georgia*, 2017, pp. 2017–228.

[19] Shark, S., Hablitzel, S., Tolentino, A., Welander, B., Jackson, J., Hall, S., Gilland, J., Jorns, B., and Hofer, R., "High Power Demonstration of a 100 kW Nested Hall Thruster System," *55th AIAA/SAE/ASEE Joint Propulsion Conference*, 2019.

[20] Mikellides, I. G., Katz, I., Hofer, R. R., and Goebel, D. M., "Magnetic shielding of a laboratory Hall thruster. I. Theory and validation," *Journal of Applied Physics*, Vol. 115, No. 4, 2014.

[21] Hofer, R. R., Goebel, D. M., Mikellides, I. G., and Katz, I., "Magnetic shielding of a laboratory Hall thruster. II. Experiments," *Journal of Applied Physics*, Vol. 115, No. 4, 2014, pp. 043304.

[22] Mikellides, I. G., Katz, I., Hofer, R. R., Goebel, D. M., De Grys, K., and Mathers, A., "Magnetic shielding of the channel walls in a Hall plasma accelerator," *Physics of Plasmas*, Vol. 18, No. 3, 2011, pp. 033501.

[23] Mikellides, I. G., Katz, I., Hofer, R. R., and Goebel, D. M., "Magnetic shielding of walls from the unmagnetized ion beam in a Hall thruster," *Applied Physics Letters*, Vol. 102, No. 2, 2013, pp. 023509.

[24] Hofer, R. R., Cusson, S. E., Lobbia, R. B., and Gallimore, A. D., "The H9 Magnetically Shielded Hall Thruster," *35th International Electric Propulsion Conference, IEPC-2017-232, Atlanta, GA*, 2017.

[25] Cusson, S. E., Hofer, R. R., Lobbia, R. B., Jorns, B. A., and Gallimore, A. D., "Performance of the H9 Magnetically Shielded Hall Thrusters," *35th International Electric Propulsion Conference, IEPC-2017-232, Atlanta, GA*, 2017.

[26] Reid, B. M., *The Influence of Neutral Flow Rate in the Operation of Hall Thrusters.*, Ph.D. thesis, 2009.

[27] Haas, J. M., Hofer, R. R., Brown, D. L., Reid, B. M., and Gallimore, A. D., "Design of the H6 Hall Thruster for High Thrust/Power Investigation," *54th JANNAF Propulsion Meeting, Denver, CO*, 2007, pp. 14–17.

[28] Hofer, R. R., *Development and characterization of high-efficiency, high-specific impulse xenon Hall thrusters*, Ph.D. thesis, University of Michigan, 2004.

[29] Hofer, R. R., Jankovsky, R. S., and Gallimore, A. D., "High-specific impulse Hall thrusters, part 1: influence of current density and magnetic field," *Journal of Propulsion and Power*, Vol. 22, No. 4, 2006, pp. 721–731.

[30] Hofer, R. R., Jankovsky, R. S., and Gallimore, A. D., "High-specific impulse Hall thrusters, part 1: influence of current density and magnetic field," *Journal of Propulsion and Power*, Vol. 22, No. 4, 2006, pp. 721–731.

[31] Hofer, R. R., Goebel, D. M., and Watkins, R. M., "Compact high current rare-earth emitter hollow cathode for hall effect thrusters," 2012, US Patent 8,143,788.

[32] Hofer, R., Goebel, D., and Watkins, R., "Compact LaB_6 Hollow Cathode for a 6-kW Hall Thruster," *54th JANNAF Propulsion Meeting*, pp. 14–17.

[33] Goebel, D., Jameson, K. K., and Hofer, R. R., "Hall thruster cathode flow impact on coupling voltage and cathode life," *Journal of Propulsion and Power*, Vol. 28, No. 2, 2012, pp. 355–363.

[34] Hofer, R. R., Johnson, L. K., Goebel, D. M., and Wirz, R. E., "Effects of internally mounted cathodes on Hall thruster plume properties," *IEEE Transactions on Plasma Science*, Vol. 36, No. 5, 2008, pp. 2004–2014.

[35] Reid, B., Gallimore, A., Hofer, R., Li, Y., and Haas, J., "Anode design and verification for a 6-kW Hall thruster," *JANNAF Journal of Propulsion and Energetics*, Vol. 3, No. 1, 2010, pp. 29–43.

[36] De Grys, K., Fisher, J., Wilson, F., Beal, B., Dimicco, J., and Khayms, V., "5 kW Hall Thruster System Qualification Status," *40th AIAA/ASME/SAE/ASEE Joint Propulsion Conference and Exhibit*, 2005, p. 3603.

[37] Goebel, D. M., Hofer, R. R., Mikellides, I. G., Katz, I., Polk, J. E., and Dotson, B. N., "Conducting wall Hall thrusters," *IEEE Transactions on Plasma Science*, Vol. 43, No. 1, 2014, pp. 118–126.

[38] Liang, R. and Gallimore, A., "Far-field plume measurements of a nested-channel hall-effect thruster," *49th AIAA Aerospace Sciences Meeting including the New Horizons Forum and Aerospace Exposition*, 2011, p. 1016.

[39] Liang, R. and Gallimore, A., "Constant-power performance and plume measurements of a nested-channel hall-effect thruster," *32nd International Electric Propulsion Conference*, 2011.

[40] Hall, S., *Characterization of a 100-kW Class Nested-Channel Hall Thruster*, Ph.D. thesis, University of Michigan, 2018.

[41] Mikellides, I. G. and Ortega, A. L., "Numerical Simulations of a 100-kW Class Nested Hall Thruster with the 2-D Axisymmetric Code Hall2De," *35th International Electric Propulsion Conference, IEPC-2017-220, Electric Rocket Propulsion Society, Atlanta, GA*, 2017.

[42] Mikellides, I. G. and Ortega, A. L., "2D (r–z) numerical simulations of the plasma and channel erosion in a 100 kW class nested Hall thruster," *Plasma Sources Science and Technology*, Vol. 27, No. 7, 2018, pp. 075001.

[43] Hofer, R. R., Polk, J. E., Sekerak, M. J., Mikellides, I. G., Kamhawi, H., Sarver-Verhey, T. R., Herman, D. A., and Williams, G., "The 12.5 kW Hall effect rocket with magnetic shielding (HERMeS) for the asteroid redirect robotic mission," *52nd AIAA/SAE/ASEE Joint Propulsion Conference*, 2016, p. 4825.

[44] Sekerak, M., Hofer, R., Polk, J., Jorns, B., and Mikellides, I., "Wear testing of a magnetically shielded hall thruster at 2000 s specific impulse," *34th International Electric Propulsion Conference, IEPC-2015-155, Kobe, Japan*, 2015.

[45] Hofer, R., Goebel, D., Mikellides, I., and Katz, I., "Design of a laboratory Hall thruster with magnetically shielded channel walls, phase II: Experiments," *48th AIAA/ASME/SAE/ASEE Joint Propulsion Conference & Exhibit*, 2012, p. 3788.

[46] Hofer, R. R., Jorns, B. A., Polk, J. E., Mikellides, I. G., and Snyder, J. S., "Wear test of a magnetically shielded Hall thruster at 3000 seconds specific impulse," *33rd International Electric Propulsion Conference*, 2013, pp. 1–24.

[47] Shastry, R., Gallimore, A., and Hofer, R., "Near-wall plasma properties and EEDF measurements of a 6-kW Hall thruster," *45th AIAA/ASME/SAE/ASEE Joint Propulsion Conference & Exhibit*, 2009, p. 5356.

[48] Jorns, B., Goebel, D. M., and Hofer, R. R., "Plasma perturbations in high-speed probing of Hall thruster discharge chambers: Quantification and mitigation," *51st AIAA/SAE/ASEE Joint Propulsion Conference*, 2015, p. 4006.

[49] Grimaud, L. and Mazouffre, S., "Performance comparison between standard and magnetically shielded 200 W Hall thrusters with BN-SiO2 and graphite channel walls," *Vacuum*, Vol. 155, 2018, pp. 514–523.

[50] Boyd, I. D., Van Gilder, D. B., and Liu, X., "Monte Carlo simulation of neutral xenon flows in electric propulsion devices," *Journal of propulsion and power*, Vol. 14, No. 6, 1998, pp. 1009–1015.

[51] Bird, G. A. and Brady, J., *Molecular gas dynamics and the direct simulation of gas flows*, Vol. 5, Clarendon press Oxford, 1994.

[52] Jorns, B., Dodson, C. A., Anderson, J. R., Goebel, D. M., Hofer, R. R., Sekerak, M. J., Lopez Ortega, A., and Mikellides, I. G., "Mechanisms for pole piece erosion in a 6-kW magnetically-shielded Hall thruster," *52nd AIAA/SAE/ASEE Joint Propulsion Conference*, 2016, p. 4839.

[53] Lopez Ortega, A., Mikellides, I. G., Sekerak, M. J., and Jorns, B. A., "Plasma simulations in 2-D (rz) geometry for the assessment of pole erosion in a magnetically shielded Hall thruster," *Journal of Applied Physics*, Vol. 125, No. 3, 2019, pp. 033302.

[54] Katz, I., Lopez Ortega, A., Goebel, D. M., Sekerak, M. J., Hofer, R. R., Jorns, B. A., and Brophy, J. R., "Effect of solar array plume interactions on Hall thruster cathode common potentials," 2016.

[55] Hofer, R. R., Jorns, B. A., Katz, I., and Brophy, J. R., "Hall effect thruster electrical configuration," 2017, US Patent App. 15/474,480.

[56] Dankanich, J. W., Walker, M., Swiatek, M. W., and Yim, J. T., "Recommended Practice for Pressure Measurement and Calculation of Effective Pumping Speed in Electric Propulsion Testing," *Journal of Propulsion and Power*, Vol. 33, No. 3, 2016, pp. 668–680.

[57] de Grys, K., Meckel, N., Callis, G., Greisen, D., Hoskins, A., King, D., Wilson, F., Werthman, L., and Khayms, V., "Development and testing of a 4500 watt flight type Hall thruster and cathode," *IEPC Paper*, 2001, pp. 01–011.

[58] Haag, T. W., "Thrust stand for high-power electric propulsion devices," *Review of Scientific Instruments*, Vol. 62, No. 5, 1991, pp. 1186–1191.

[59] Xu, K. G. and Walker, M. L., "High-power, null-type, inverted pendulum thrust stand," *Review of Scientific Instruments*, Vol. 80, No. 5, 2009, pp. 055103.

[60] Cusson, S. E. and Jorns, B. A., "Non-invasive in-situ measurement of the near-wall ion kinetic energy in a magnetically shielded Hall thruster," *Plasma Science Sources and Technology*, 2019 (Submitted).

[61] Jorns, B. A. and Hofer, R. R., "Plasma oscillations in a 6-kW magnetically shielded Hall thruster," *Physics of Plasmas*, Vol. 21, No. 5, 2014, pp. 053512.

[62] Jorns, B. A. and Hofer, R. R., "Low frequency plasma oscillations in a 6-kW magnetically shielded hall thruster," *49th AIAA/ASME/SAE/ASEE Joint PropulsionConference*, 2013, p. 4119.

[63] Hofer, R. R. and Anderson, J. R., "Finite pressure effects in magnetically shielded Hall thrusters," *50th AIAA/ASME/SAE/ASEE Joint Propulsion Conference*, 2014, p. 3709.